Neuron
Article

Dynamic Encoding of Perception, Memory, and Movement in a *C. elegans* Chemotaxis Circuit

Linjiao Luo,[1,2,3,9] Quan Wen,[2,3,7,9] Jing Ren,[2,4,9] Michael Hendricks,[2,4,8,9] Marc Gershow,[2,3] Yuqi Qin,[2,4] Joel Greenwood,[2] Edward R. Soucy,[2] Mason Klein,[2,3] Heidi K. Smith-Parker,[5] Ana C. Calvo,[6] Daniel A. Colón-Ramos,[6] Aravinthan D.T. Samuel,[2,3,*] and Yun Zhang[2,4,*]

[1]Key Laboratory of Modern Acoustics, Ministry of Education, Department of Physics, Nanjing University, China
[2]Center for Brain Science
[3]Department of Physics
[4]Department of Organismic and Evolutionary Biology
Harvard University, Cambridge, MA 02138, USA
[5]Department of Biochemistry and Molecular Biophysics, Columbia University, New York, NY 10032, USA
[6]Program in Cellular Neuroscience, Neurodegeneration and Repair, Department of Cell Biology, Yale University School of Medicine, New Haven, CT 06536, USA
[7]Department of Neurobiology and Biophysics, School of Life Sciences, University of Science and Technology of China, China
[8]Present address: Department of Biology, McGill University, Montreal, QC, H3A 1B1, Canada
[9]Co-first authors
*Correspondence: samuel@physics.harvard.edu (A.D.T.S.), yzhang@oeb.harvard.edu (Y.Z.)
http://dx.doi.org/10.1016/j.neuron.2014.05.010

SUMMARY

Brain circuits endow behavioral flexibility. Here, we study circuits encoding flexible chemotaxis in *C. elegans*, where the animal navigates up or down NaCl gradients (positive or negative chemotaxis) to reach the salt concentration of previous growth (the set point). The ASER sensory neuron mediates positive and negative chemotaxis by regulating the frequency and direction of reorientation movements in response to salt gradients. Both salt gradients and set point memory are encoded in ASER temporal activity patterns. Distinct temporal activity patterns in interneurons immediately downstream of ASER encode chemotactic movement decisions. Different interneuron combinations regulate positive versus negative chemotaxis. We conclude that sensorimotor pathways are segregated immediately after the primary sensory neuron in the chemotaxis circuit, and sensory representation is rapidly transformed to motor representation at the first interneuron layer. Our study reveals compact encoding of perception, memory, and locomotion in an experience-dependent navigational behavior in *C. elegans*.

INTRODUCTION

Brain circuits endow animals with flexibility to drive learned behaviors, requiring that multiple patterns of sensory, memory, and motor activities can be encoded and organized in the nervous system connectome. Because synaptic connectivity can be ambiguous about information flow, functional analysis is required to characterize circuit mechanisms for perception, memory, and motor activities that underlie learned behaviors. Here, we address these questions in experience-dependent chemotaxis in the nematode *C. elegans*.

C. elegans exhibits chemotaxis toward numerous compounds, including NaCl (Bargmann and Horvitz, 1991; Ward, 1973). It was shown that *C. elegans* is attracted to higher NaCl concentrations. This behavioral response can be modulated by associative learning between specific salt concentration and starvation, suggesting that salt chemotaxis is used to help locate food (Saeki et al., 2001; Tomioka et al., 2006). Preexposure to high salt concentrations attenuates salt chemotaxis, suggesting that salt perception also exhibits habituation (Jansen et al., 2002). However, salinity is not only a sensory cue but also an environmental factor, like temperature, that directly affects cell physiology; either too high or too low NaCl concentrations could be undesirable. For small animals like *C. elegans*, adaptation to environmental conditions can be partly met through motile behavior. For example, the animal can actively migrate toward a specific temperature to which it has become accustomed, irrespective of whether the animal is fed or starved at that temperature (Ramot et al., 2008).

We refer to movement up or down salt gradients as positive or negative chemotaxis, respectively. Previous studies revealed the sensory neurons and behavioral strategies underlying positive salt chemotaxis (Iino and Yoshida, 2009; Pierce-Shimomura et al., 1999; Ward, 1973). Through laser ablation analysis, Bargmann and Horvitz (1991) discovered that the ASE neurons represent the principal sensory neurons for attraction toward NaCl. The left-right pair of ASE neurons (ASEL and ASER, respectively) (Figure 1A) exhibit asymmetries in gene expression, developmental programs, and physiological properties (Chang et al., 2003; Pierce-Shimomura et al., 2001; Suzuki et al., 2008). The ASEL/R neurons connect with several postsynaptic interneurons with a complex pattern, where the same sensory neuron simultaneously connects with multiple interneurons, principally the AIY, AIZ, and AIB interneurons, that also interconnect with each other

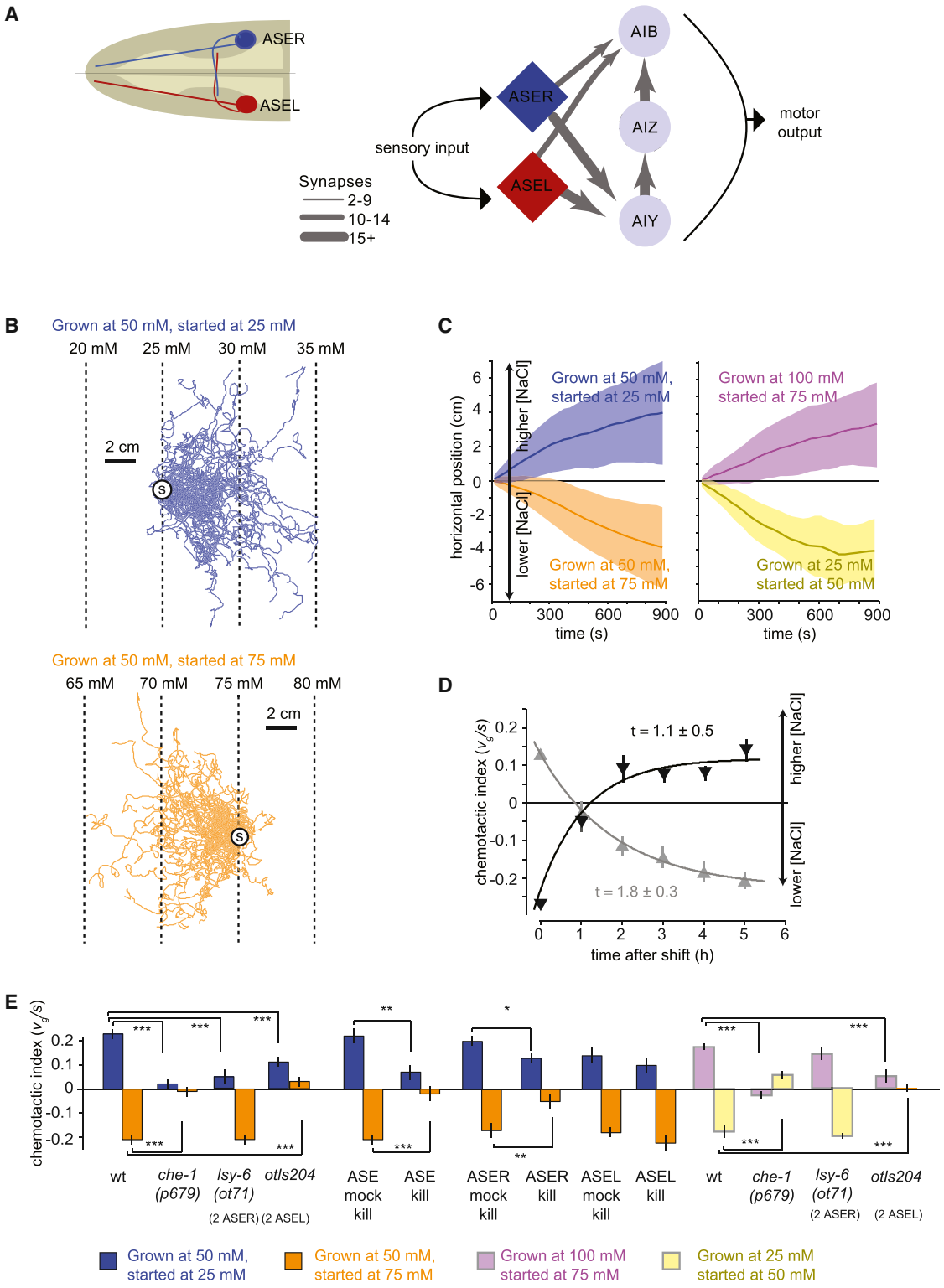

Figure 1. *C. elegans* Performs Bidirectional Chemotaxis in Linear NaCl Gradients

(A) Simplified synaptic connections for the salt-sensing ASE neurons.

(B) Navigation trajectories of 50 wild-type N2 animals on linear NaCl gradients with 2 mM NaCl/cm steepness. Animals were grown at 50 mM NaCl and started at 25 mM (blue) or 75 mM (orange). Trajectories are aligned to have the same starting point (circle with S) for presentation purposes.

(legend continued on next page)

(Figure 1A) (White et al., 1986). By tracking the movements of individual worms moving up NaCl gradients, Pierce-Shimomura et al. (1999) showed that a biased random walk strategy contributes to positive chemotaxis. In isotropic environments, periods of forward movement (runs) are interrupted by rapid reorientations (turns and reversals). During chemotaxis up NaCl gradients, transient increases (or decreases) in local salt concentration will lengthen (or shorten) runs, increasing the time spent crawling toward higher NaCl concentrations. Iino and Yoshida (2009) showed that *C. elegans* also augments chemotaxis by actively orienting forward movement toward higher salt concentrations. Active orientation toward preferred environments is called a klinotaxis or "weathervaning" strategy. Thus, chemotaxis involves two strategies, a biased random walk and klinotaxis.

The physiological responses of the ASE neurons have been proposed to encode the preference for higher salt concentrations (Suzuki et al., 2008; Thiele et al., 2009). ASEL and ASER are activated by upsteps and downsteps in NaCl concentration, respectively. Binary patterns of step-evoked activity inspired circuit models that reflexively translate the ON/OFF activity patterns of sensory neurons to downstream interneurons to drive movements up salt gradients. A biased random walk up salt gradient would arise when runs are lengthened (i.e., reorientation frequency is lowered) in response to ASEL activity but runs are shortened (i.e., reorientation frequency is raised) in response to ASER activity. The ADF and ASH sensory neurons also have similar step-evoked physiological responses as ASE but are less significant for chemotactic behavior.

However, positive chemotaxis is one product of a more flexible chemotaxis circuit. On smooth gradients of salt concentration, *C. elegans* will navigate up or down salt gradients toward salt concentrations corresponding to previous growth conditions (Kunitomo et al., 2013), suggesting a more sophisticated encoding of perception, memory, and motor behaviors in the chemotactic circuit. The valence of a given salt gradient —whether the worm prefers to move up or down the gradient toward higher or lower salt concentrations —depends on comparison between the current conditions and the remembered set point. Mapping perception, memory, and motor performance from sensory neurons to downstream interneuron pathways is critical for understanding how the nervous system encodes behavioral flexibility. Here, we combine quantitative behavioral analysis, optogenetics, targeted cell inactivation, and calcium imaging from sensory neurons to interneurons in restrained and freely moving worms to illuminate how the chemotaxis circuit generates experience-dependent navigation.

We found that *C. elegans* ascends or descends salt gradients in an experience-dependent way by using strikingly symmetric behavioral strategies. In both cases, the single ASER sensory neuron is essential. While ASER calcium transients are activated or suppressed by decreasing or increasing NaCl concentration during positive chemotaxis below the set point or negative chemotaxis above the set point, the temporal profiles of ASER activities differ between each condition. Thus, both the perception of the ambient salt gradient and the memory of the chemotactic set point can be inferred from ASER neuronal dynamics. Downstream of ASER, the pathways for positive versus negative chemotaxis and pathways for regulating the frequency versus the direction of reorientation movements are distributed and rapidly segregated at the first interneuron layer. Divergence generates a circuit layout that is flexible and robust to perturbation, supporting experience-dependent chemotaxis as well as distinct components of navigational strategy. We also discovered multiple encoding schemes for navigational movement among interneurons. The temporal dynamics of individual interneurons are direct representations of chemotactic movement but not sensory input or memory, revealing a surprisingly rapid transformation from sensory representation to motor representation in the first relay of the navigational circuit. Multiple mechanisms, such as modulation of synaptic strength or alternative engagement of distinct circuits, can contribute to flexibility of neural circuits and to generation of optimal behavior in response to environmental conditions (Ha et al., 2010; Herry et al., 2008; Jing and Gillette, 2000; Kerchner and Nicoll, 2008). Our results provide insights into how a complex experience-dependent behavior can be compactly encoded in the small anatomical connectome of *C. elegans*.

RESULTS

C. elegans Performs Experience-Dependent Salt Chemotaxis

We use high-pixel density cameras to record the movements of individual young adult worms performing chemotaxis across 25 cm × 25 cm agar plates. Large space for chemotaxis allows us to study many worms at once. Because the worms are placed on the plates at low density, they rarely collide with one another or with the plate boundaries, generating many uninterrupted trajectories of individual worms performing chemotaxis in each experiment. We also use a simple method to generate stable, precise linear NaCl gradients on these agar plates without osmolarity gradients (Figure S1 available online).

(C) Average horizontal position of worms grown at specific salt concentrations and started at different salt concentrations on 2 mM/cM NaCl steepness linear gradients as shown in (B). Solid lines and shading indicate the mean ±1 STD of horizontal displacement from the start point over time measured over the trajectories of individual worms. Positive horizontal displacement is toward higher salt concentrations in all panels. n > 280 animals for each measurement.
(D) Upshift (dark gray) and downshift (light gray) of navigational indexes for wild-type N2 animals grown overnight at one salt concentration (50 or 100 mM NaCl, respectively) and then shifted to a new salt concentration (100 mM or 50 mM NaCl, respectively) for a specified time interval before being placed on a 2 mM/cm linear NaCl gradient at 75 mM (n > 40 animals for each measurement). The chemotactic index, the ratio between the velocity of each trajectory in the horizontal direction divided by the crawling speed along each trajectory, $\langle v_g \rangle / \langle s \rangle$, was computed. Each data point represents mean ±SEM. Solid lines represent least-squares fits to exponential time courses. The time constant of each exponential fit ±SD is shown.
(E) Chemotactic indexes of wild-type, mutant, ASE laser-killed animals, and ASE mock surgical controls in linear 2 mM/cm NaCl gradients. ANOVA Tukey-Kramer post hoc was used to compare wild-type and mutants. Student's t test was used to compare laser-killed animals with mock surgical controls. ***p < 0.0005; **p < 0.005. n > 20 animals for each measurement. Data points represent mean ±SEM.

When *C. elegans* is cultivated at 50 mM NaCl and placed on linear salt gradients (2 mM/cm), worms crawl toward higher NaCl concentrations when started at 25 mM NaCl but toward lower concentrations when started at 75 mM NaCl (Figure 1B). Thus, positive chemotaxis up salt gradients is one component of a more versatile chemotaxis circuit. We also asked how chemotaxis is modulated by experience. Worms grown at 100 mM NaCl and started at 75 mM NaCl crawl toward higher NaCl concentrations; worms grown at 25 mM NaCl and started at 50 mM NaCl crawl toward lower NaCl concentrations (Figure 1C). These observations indicate that the set point is experience dependent. When worms reach the salt concentration corresponding to previous growth, they move randomly, without drifting up or down the gradient (data not shown).

To determine whether chemotactic preference retains adult stage plasticity, we grew worms at 100 mM NaCl and transferred them as young adults to cultivation plates with 50 mM NaCl with food before starting them at 75 mM NaCl on linear gradients (Figure 1D). To quantify chemotactic rate and direction, we use a nondimensional index based on individual trajectories: the mean velocity of the trajectories along the gradient direction, $\langle v_g \rangle$, divided by the mean crawling speed along the trajectory, $\langle s \rangle$. Thus, if all worms crawled straight up or down gradients, the index would be +1 or −1, respectively. If worms moved randomly, the index would be near 0. With no retraining at 50 mM, worms crawled up NaCl gradients. After several hours' retraining, worms crawled down gradients with nearly the same index as worms grown overnight at 50 mM NaCl (Figure 1D). Similarly, by growing worms overnight at 50 mM NaCl and transferring them to plates with 100 mM NaCl and food, the set point gradually shifted to 100 mM. The learning curves for raising or lowering the set point exhibit similar exponential time courses (Figure 1D).

The ASER Neuron Is Required for Both Positive and Negative Salt Chemotaxis

The ASE neurons have been shown to contribute to positive chemotaxis (Bargmann and Horvitz, 1991; Suzuki et al., 2008). The loss-of-function mutation in the *che-1* transcription factor, *che-1*(*p679*), specifically disrupts the development of both ASE neurons and abolishes positive salt chemotaxis (Uchida et al., 2003). We found that the *che-1*(*p679*) mutation abolished chemotaxis toward different set points (25 mM, 50 mM, and 100 mM) from higher or lower salt concentrations (Figure 1E). Laser ablation of both ASE neurons disrupted salt chemotaxis (Figure 1E).

The ASEL and ASER neurons show asymmetries in gene expression and physiological properties (Chang et al., 2003; Johnston and Hobert, 2003; Suzuki et al., 2008). We found that killing the ASER neuron disrupted both positive and negative chemotaxis, whereas killing the ASEL neuron had no measurable effect (Figure 1E). Thus, ASER plays the critical role in both positive and negative chemotaxis. We further explored the requirement of ASER using the *lsy-6*(*ot71*) mutant where both ASE neurons adopt the ASER cell fate and the *otIs204* transgenic line where both ASE neurons adopt the ASEL cell fate (Johnston and Hobert, 2003). Animals with two ASER neurons (i.e., no ASEL neuron) were capable of exhibiting both positive and negative chemotaxis toward different set points, whereas animals with two ASEL neurons (i.e., no ASER neuron) were not capable of oriented movement toward the salt concentration of previous growth (Figure 1E). These results further support ASER's role in encoding the chemotactic set point as well as responding to the salt gradient during both positive and negative chemotaxis.

The Same Behavior Strategies Underlie Positive and Negative Chemotaxis

C. elegans navigation involves successive forward movements (runs) interrupted at random by reorientation movements (sharp turns or reversal-turns) (Figure 2A). Previous studies on positive chemotaxis have shown that the worm extends runs up gradients and shortens runs down gradients, thereby biasing a random walk toward higher salt concentrations (Pierce-Shimomura et al., 1999). In addition, worms actively orient themselves up salt gradients, a strategy called klinotaxis or weathervaning (Iino and Yoshida, 2009). Linear gradients allowed us to easily identify runs and reorientation movements along each trajectory that were directed up, down, or orthogonal to the gradient. We used this setup to dissect movement patterns during positive and negative chemotaxis.

First, we examined the statistics of run durations, the time intervals between successive reorientation movements. During positive and negative chemotaxis, we found that the worm biases its random walk with mirror symmetry in response to gradient direction (Figures 2B and 2D). Runs pointed toward the preferred direction (up gradients during positive chemotaxis or down gradients during negative chemotaxis) are longer than runs orthogonal to the gradient. Runs pointed away from the preferred direction are shorter than orthogonal runs (Figures 2B and 2D). Our results confirm reports that the worm both extends runs up gradients and shortens runs down gradients during positive chemotaxis. The worm also extends runs down gradients and shortens runs up gradients during negative chemotaxis. These analyses demonstrate that the neural circuit for chemotaxis must encode whether the worm is moving up or down a salt gradient as well as whether it is above or below its chemotactic set point.

Next, we sought the types of reorientation movement contributing to klinotaxis. We looked for biases in directional changes during runs or after sharp turns or reversal-turns during chemotaxis. During runs orthogonal to the gradient, we found that worms gradually veer toward the preferred and nonpreferred directions by similar amounts (Figures 2C and 2E). However, sharp turns after these orthogonal runs are more likely to point toward the preferred direction (Figures 2C and 2E). Reversal-turns after orthogonal runs are not more likely to reorient the worm toward preferred directions. The tendency to turn toward preferred chemical environments has been observed in microfluidic devices with step gradients of chemoattractants in fluid streams (Albrecht and Bargmann, 2011; McCormick et al., 2011). Klinotaxis in linear spatial gradients arises from sharp turns during both positive and negative salt chemotaxis.

ASER Neuronal Dynamics Encode Both Gradient Perception and Set Point Memory

To further characterize ASER function, we performed intracellular calcium imaging. The physiological properties of the ASE

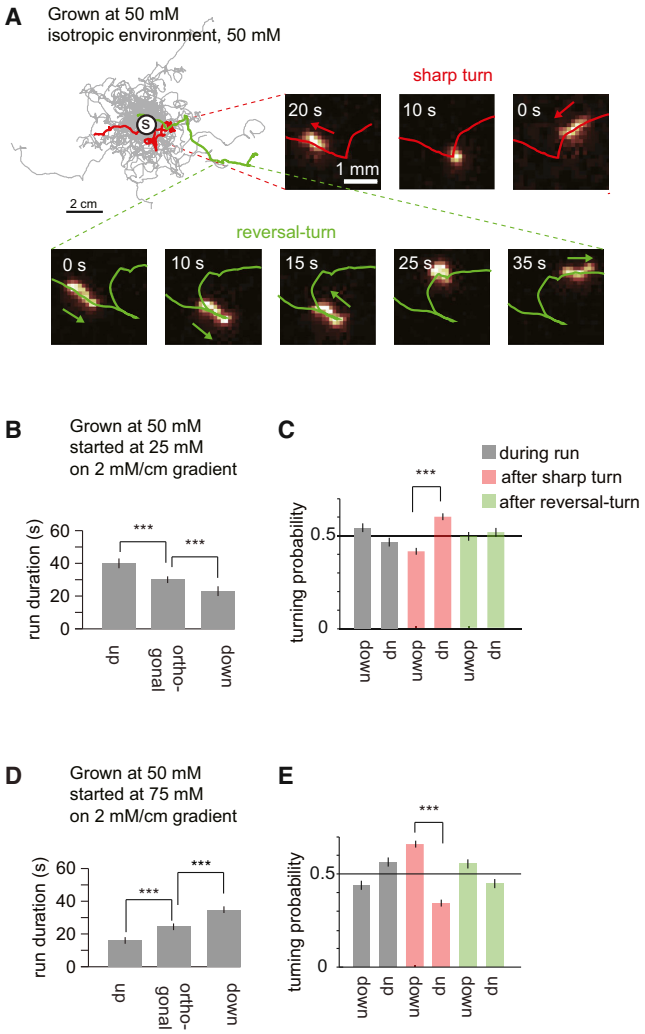

Figure 2. A Biased Random Walk Underlies Both Positive and Negative Chemotaxis

(A) Navigation trajectories of 50 wild-type N2 animals in isotropic environment of 50 mM NaCl. Worms were grown with 50mM of NaCl and trajectories were aligned to have the same starting point (circle with S). Two series of video frames show a flagged sharp turn and a reversal-turn.

(B and D) Run durations for navigation in linear 2 mM/cm NaCl gradients for worms exhibiting positive chemotaxis below the set point (B) or negative chemotaxis above the set point (D). The direction up the gradient is 0°. Runs up: runs with mean headings between −22.5° and +22.5°. Runs down: runs with mean headings <−157.5° or >+157.50°. Runs orthogonal: runs with headings between −112.5° and −67.5° or between +67.5° and +112.5°. Run durations are compared using ANOVA Tukey-Kramer post hoc; ***$p < 0.0005$. Error bars denote SEM; n = 280 animals.

(C and E) Probabilities of reorientation up or down the gradient after orthogonal runs during positive chemotaxis ([C], n = 280 animals grown at 50 mM) or negative chemotaxis ([E], n = 300 animals grown at 50 mM). Two-sample z test; ***$p < 0.0005$; error bars denote SEM.

neurons have been explored using step changes in salt concentration (Kunitomo et al., 2013; Suzuki et al., 2008). ASER was shown to be an "OFF" neuron that is activated by downsteps in NaCl concentration. ASEL was shown to be an "ON" neuron that is activated by upsteps in NaCl concentration. These results suggested a model where binary ASE activity patterns are reflexively mapped to downstream neurons to either stimulate or suppress turning movements, driving a biased random walk up gradients.

We quantified calcium dynamics in ASEL and ASER in worms that were grown at 50 mM NaCl and subjected to small step changes in NaCl concentration (±5 mM) above or below the set point (Figures S2A–S2D). We measured the calcium transients in transgenic animals that expressed the calcium-sensitive protein GCaMP3.3 (Tian et al., 2009) specifically in ASE. Consistent with prior reports, intracellular calcium levels in ASEL and ASER increased after upsteps and downsteps in NaCl concentration, respectively, whether above or below the set point (Figures S2A–S2D). The fixed calcium dynamics of ASER neurons to step stimuli, combined with the fact that ASER drives both positive and negative chemotaxis, suggests flexible coupling between ASER activity and behavioral output. To determine whether ASER can generate flexible behavioral outputs, we expressed channelrhodopsin specifically in the ASER neurons of worms that carried a mutation in the *lite-1* gene that eliminated the endogenous turning response to blue light (Boyden et al., 2005; Edwards et al., 2008; Liu et al., 2010). We subjected freely moving worms raised at 50 mM NaCl to short pulses of blue light in environments both above (75 mM) and below (25 mM) their set point. We found that optogenetic activation of the ASER neuron triggered a transient increase in reorientation rate for animals below the set point but a transient decrease when above the set point (Figure S2E). Thus, ASER activity is connected to an increase in reorientation rate during positive chemotaxis but is connected to a decrease in reorientation rate during negative chemotaxis. Thus, ASER must encode both the perception of salt gradients and the memory of the chemotactic set point.

We reasoned that step stimuli might saturate ASER calcium levels, making it difficult to resolve stimulus- or memory-dependent contrasts in ASER neuronal dynamics; 5 mM step changes in salt concentration (the smallest steps that we could reliably deliver with our microfluidic setup) are much larger than the salt gradients encountered by moving worms in our behavioral setup and also lack the property of smoothly varying salt concentrations of our behavioral assay. To see whether ASER activity patterns might reflect both perception and memory with behaviorally relevant stimuli, we analyzed ASER calcium dynamics in response to linear temporal gradients of salt concentrations that were comparable (83 ± 5 μM/s) to gradients experienced in our behavioral setup. Thus, we designed a mixing chamber for our microfluidic imaging device that allowed us to subject worms to linearly varying salt concentrations (Figure S3).

Using linear salt gradients, we found that ASER's detailed temporal dynamics jointly depend on the sign of the stimulus gradient (increasing or decreasing NaCl concentration) and whether the animal is above or below the chemotactic set point. We cultivated animals to generate a 50 mM NaCl set point. When animals were exposed to a linear decrease in salt concentration below the set point, ASER exhibited large, sustained calcium waves that persisted for as long as the gradient was applied (Figure 3A). When these animals were exposed to a linear increase in salt concentration below the set point, ASER activity was

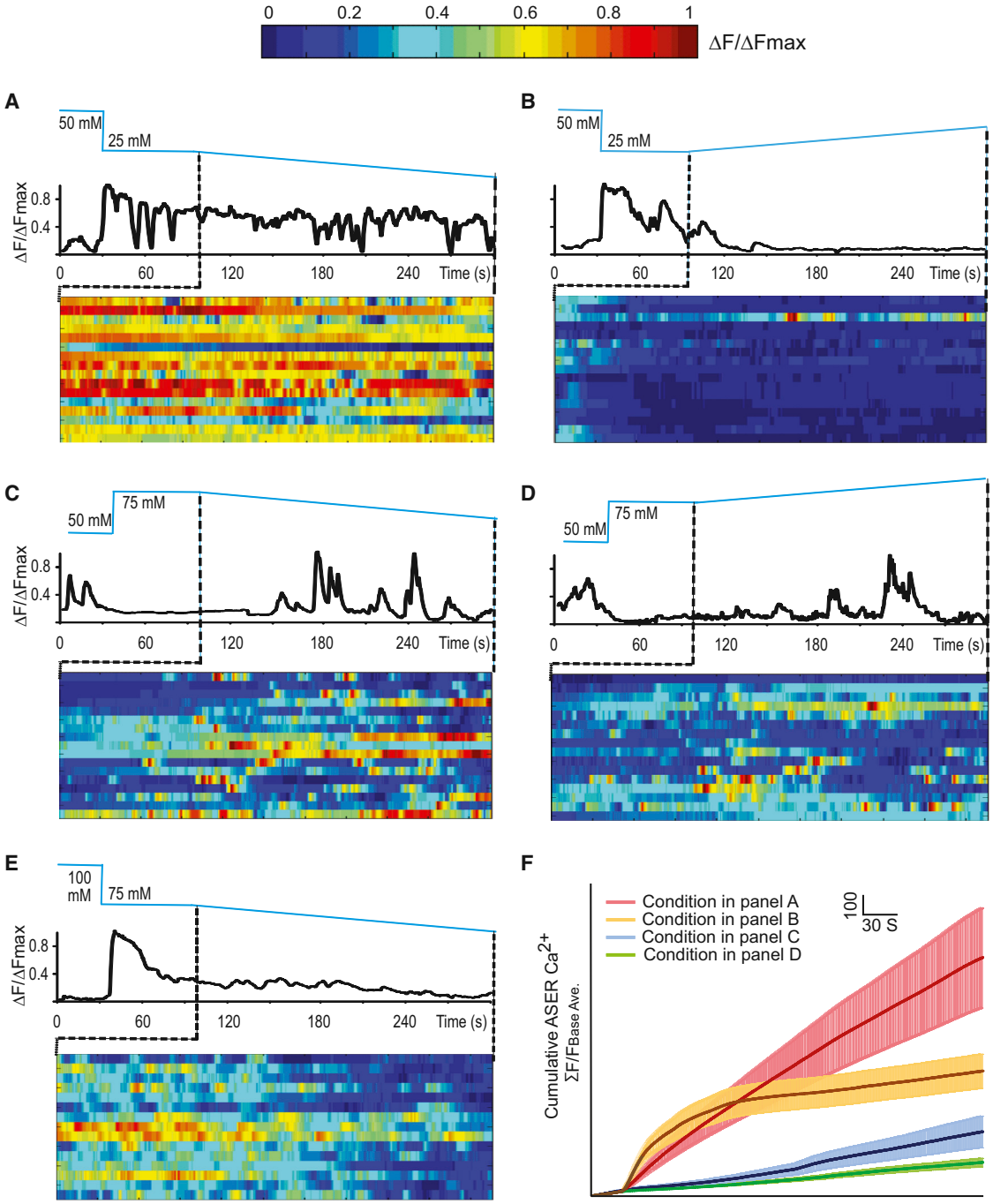

Figure 3. ASER Calcium Imaging in Response to Salt Gradients Delivered by Microfluidic Device

(A–E) Sample traces of GCaMP3 in ASER in one animal and the heatmaps of GCaMP3 in ASER in multiple animals that raised at 50 mM NaCl responding to a decreasing gradient of NaCl starting at 25 mM (A), raised at 50 mM responding to an increasing salt gradient starting at 25 mM NaCl (B), raised at 50 mM responding to a decreasing salt gradient starting at 75 mM NaCl (C), raised at 50 mM responding to an increasing salt gradient starting at 75 mM NaCl (D), or raised at 100 mM NaCl responding to a decreasing salt gradient starting at 75 mM NaCl (E).

To calculate $\Delta F/\Delta F_{max}$ ([A]–[E]), we subtracted the calcium intensity of each time point (F) by the minimal calcium intensity of the time series (F_{min}) and divided the difference by the difference between the maximal (F_{max}) and minimal (F_{min}) calcium intensity of the time series ($\Delta F/\Delta F_{max} = (F-F_{min})/(F_{max}-F_{min})$).

(F) Cumulative GCaMP3 signal in ASER neurons as shown in (A)–(D). Solid lines and shadings are mean ±SEM. n > 15 animals under each condition. To calculate the cumulative calcium intensity for each time point, we divided the sum of the calcium intensity from time zero to the current time point by the average calcium intensity during the baseline period (i.e., the first 30 s).

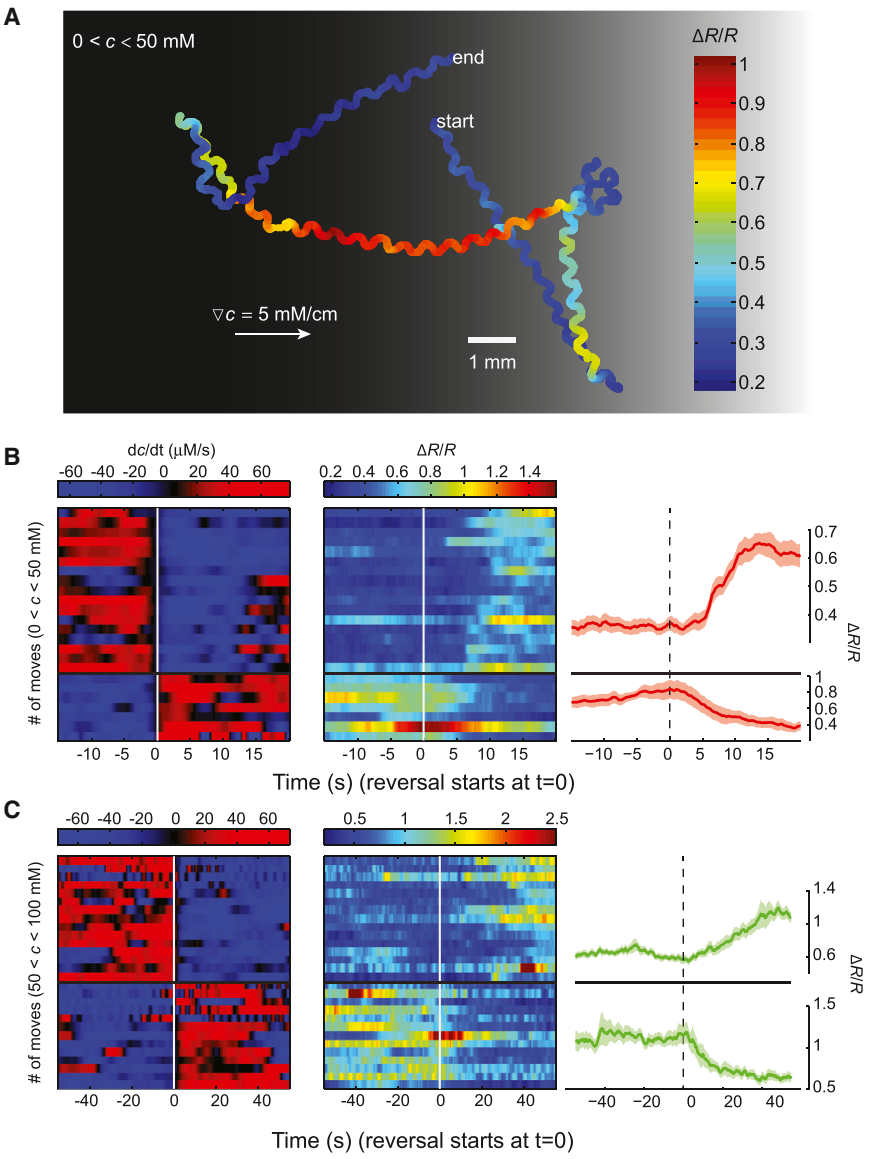

Figure 4. ASER Calcium Imaging in Freely Navigating Worms

(A) Representative ASER motion trajectory as well as its ratiometric calcium signal (R) in a worm freely navigating a linear salt gradient. ASER exhibited higher level of calcium activity when the worm moved down the gradient (toward left).

(B and C) Heatmap and mean values of ASER calcium dynamics when *C. elegans* navigates below (B) or above (C) the set point (50 mM NaCl). Left and middle panels: temporal salt gradient experienced by worms during reversals and/or turns (left panels, rows) and the corresponding calcium signals in ASER (middle panels). Right panels: mean values of ASER ratiometric calcium signals during transitions from moving up the gradient ($dC/dt > 0$) to moving down the gradient ($dC/dt < 0$) and vice versa. A total of 24 events from n = 10 animals (B) and 28 events from n = 10 animals (C) are shown; mean ±SEM.

completely suppressed (Figure 3B). In contrast, when worms were exposed to the same decreasing or increasing gradients above the set point, ASER exhibited different activity patterns. Decreasing salt concentration evoked sustained as well as short and discrete calcium transients that were separated by periods of inactivity (Figure 3C). Increasing salt concentration evoked short and discrete calcium transients at a lower frequency (Figure 3D). These results indicate that both set point memory and gradient perception can be inferred from ASER activity patterns. Whether above or below the set point, decreasing salt concentration generates more overall activity than increasing salt concentration (Figure 3F). Set point memory can be inferred from the distinct pattern of fast calcium transients that occur with greater frequency above the set point than below the set point. To further test whether ASER temporal dynamics is a function of both gradient perception and set point memory, we compared ASER activity pattern in worms with different set points. We recorded ASER in animals that were raised at 100 mM NaCl and subjected to a linear decrease of NaCl concentration at 75 mM (below the set point). The ASER activity pattern in these animals closely resembled those in animals grown at 50 mM and subjected to the same change at 25 mM NaCl concentration (below the set point) by displaying more sustained calcium transients (Figure 3E), which were less frequent in animals grown at 50 mM and subjected to the same change at 75 mM (above the set point). The richness of ASER calcium dynamics revealed by linear gradients reveals a dual role in encoding perception and memory.

We also asked whether ASER activity patterns are derived from neural circuit function. We addressed this question by examining ASER calcium transients in *unc-13*(*e51*) and *unc-31*(*e928*) mutants defective in the release of neurotransmitters and peptides, respectively (Ann et al., 1997; Avery et al., 1993; Richmond et al., 1999). We found that the perception- and memory-dependent ASER calcium dynamics were not strongly altered by missing signaling between neurons in either *unc-13* or *unc-31* mutants (Figures S4A–S4D). Thus, the temporal profiles of the ASER calcium transients that reflect both gradient perception and set point memory are largely cell autonomous.

Rapid Transformation of Sensory Representation to Motor Representation in the Salt Chemotaxis Circuit

To better understand how sensory inputs are translated into motor outputs during chemotaxis, we turned to calcium imaging in freely behaving animals. First, we used a tracking microscope to simultaneously measure ASER calcium signals and locomotion in individual animals (Figure 4A). The salt gradient

experienced by each animal was calculated based on the direction and speed of the head with respect to the direction and steepness of the ambient linear spatial salt gradient. Measuring ASER activity patterns in freely moving animals recapitulated our results using linear salt gradients with microfluidics (Figures 4B and 4C). In freely moving animals, ASER is activated by decreasing salt concentrations and inhibited by increasing salt concentrations whether above or below the set point. Sharp, discrete calcium transients appear when navigating above the set point. Signatures of both perception and memory can be inferred from ASER activity patterns in freely moving worms. We examined ASER activity patterns at all reversal points during overall trajectories and found that whereas ASER activity patterns were directly correlated with the gradient of NaCl concentration, they were not directly correlated with the direction of worm movement. ASER activity can either increase or decrease during a reversal (Figures 4B and 4C; traces are aligned such that $t = 0$ indicates when a reversal-turn is initiated). Thus, ASER activity patterns are a direct representation of sensory input and memory but are not a direct representation of chemotactic movement. The transformation of sensory representation to motor representation during chemotaxis must occur downstream of ASER.

Next, we turned our tracking microscope to postsynaptic interneurons. Several interneurons that are postsynaptic of ASER play important roles in *C. elegans* navigation, including AIB, AIY, and AIZ (Figure 1A) (White et al., 1986). Ablations of these neurons modulate the turning rates of worms in isotropic environments (Gray et al., 2005; Tsalik and Hobert, 2003), suggesting that they might regulate reorientation movements during navigation. We used cell-specific promoters to label two major postsynaptic interneurons, AIB and AIY, with the improved calcium indicator GCaMP6 (Chen et al., 2013), which enabled us to track calcium dynamics in unrestrained animals during chemotaxis (Figure 5). We also examined the command interneuron AVA, which is postsynaptic to AIB. AVA activity is directly correlated with reversals (Chronis et al., 2007; Faumont et al., 2011).

Interestingly, we found that these interneurons exhibited activity patterns that were directly correlated with reorientation movements. Each interneuron exhibited distinct temporal dynamics, suggesting multiple encoding schemes for chemotactic movements. Consistent with other studies of AVA in freely moving animals (Faumont et al., 2011), we found that the onset of a reversal was correlated with a rapid step-like rise in AVA calcium activity. AVA activity was sustained throughout the reversal and began to decline to baseline levels at the resumption of forward movement (Figure 5D). We found that AIB also encoded reorientation maneuvers during chemotaxis, but with different temporal dynamics. At the onset of a reversal, AIB calcium levels increased linearly until reaching a peak at the resumption of forward movement (Figures 5A and 5B). With the resumption of forward movement, AIB calcium levels gradually returned to baseline (Figure 5C). Whereas AVA activity rapidly peaked near the beginning of each reorientation maneuver, AIB activity peaked at the end (Figures 5B and 5C). Comparing AIB activity patterns in worms moving up or down salt gradients above or below the set point, we found that AIB activity patterns were not a direct representation of sensory input or memory (i.e., not a direct representation of ASER activity). AIB activity patterns represent motor output.

AIY activity patterns are also correlated with reorientation movements, but in a manner that is distinct from AIB or AVA. AIY calcium levels decreased at the onset of each reversal (Figures 5E and 5F). Along each chemotactic trajectory, low AIY activity was correlated with frequent reversals and slow dispersal whereas high AIY activity was correlated with long runs and rapid dispersal (Figure 5G). Our discovery that high and low levels of AIY activity in freely behaving animals is correlated with runs and reorientation movements, respectively, is consistent with laser killing analyses of AIY (Gray et al., 2005; Tsalik and Hobert, 2003). Killing AIY shortens runs and increases the reorientation rate of freely behaving animals.

Taken together, our results reveal surprisingly complex intracellular calcium dynamics of the salt chemotactic circuit. We show that within the circuit, varying temporal patterns of the ASER calcium transients represent both the current sensory stimuli as well as the memory of the sensory experience. At downstream levels, different interneurons encode distinct chemotactic maneuvers with distinct profiles of calcium activity. These results suggest rapid transformation of sensory representation to motor representation in the circuits for navigation, revealing functional strategies that a small neural circuit uses to encode perception, memory, and chemotactic movements.

Segregation of Sensorimotor Pathways for Positive and Negative Chemotaxis

Our discovery that different interneurons are correlated with motor outputs in different ways suggests a highly divergent organizational pattern in the circuits for navigation. To investigate this hypothesis, we examined behavioral effects of systematic inactivation of downstream interneurons. First, we used laser ablation to kill the main ASER postsynaptic interneurons individually or in different combinations and assessed chemotaxis in linear gradients (Figure 6). We tested worms in which sets of interneurons were ablated along with mock surgical controls for chemotaxis toward 50 mM NaCl. We found that individually ablating the AIZ or AIY interneurons had essentially no effect on chemotaxis toward the set point (Figure 6). We also examined the *ttx-3*(*ks5*) mutants, in which AIY fails to develop properly (Hobert et al., 1997). The *ttx-3* mutants exhibited wild-type chemotaxis, phenocopying the result of laser ablating AIY. We found that laser ablating AIB significantly weakened negative chemotaxis but not positive chemotaxis (Figure 6). Consistently, genetic ablation of AIB by ectopically expressing the cell-death-inducing molecule caspase generated similar effects on the chemotaxis. Another postsynaptic interneuron AIA has been recently shown to modulate the activity dynamics of the olfactory sensory neuron AWC (Chalasani et al., 2010). Ablating AIA did not significantly affect salt chemotaxis in either direction.

Although ablating single neuron types had modest effects on chemotaxis, ablating combinations of interneuron types had extensive effects (Figure 6). Ablating both AIY and AIZ disrupted both positive and negative chemotaxis, whereas ablation of AIY or AIZ alone did not disrupt either positive or negative chemotaxis. AIB ablation by itself disrupted negative chemotaxis but,

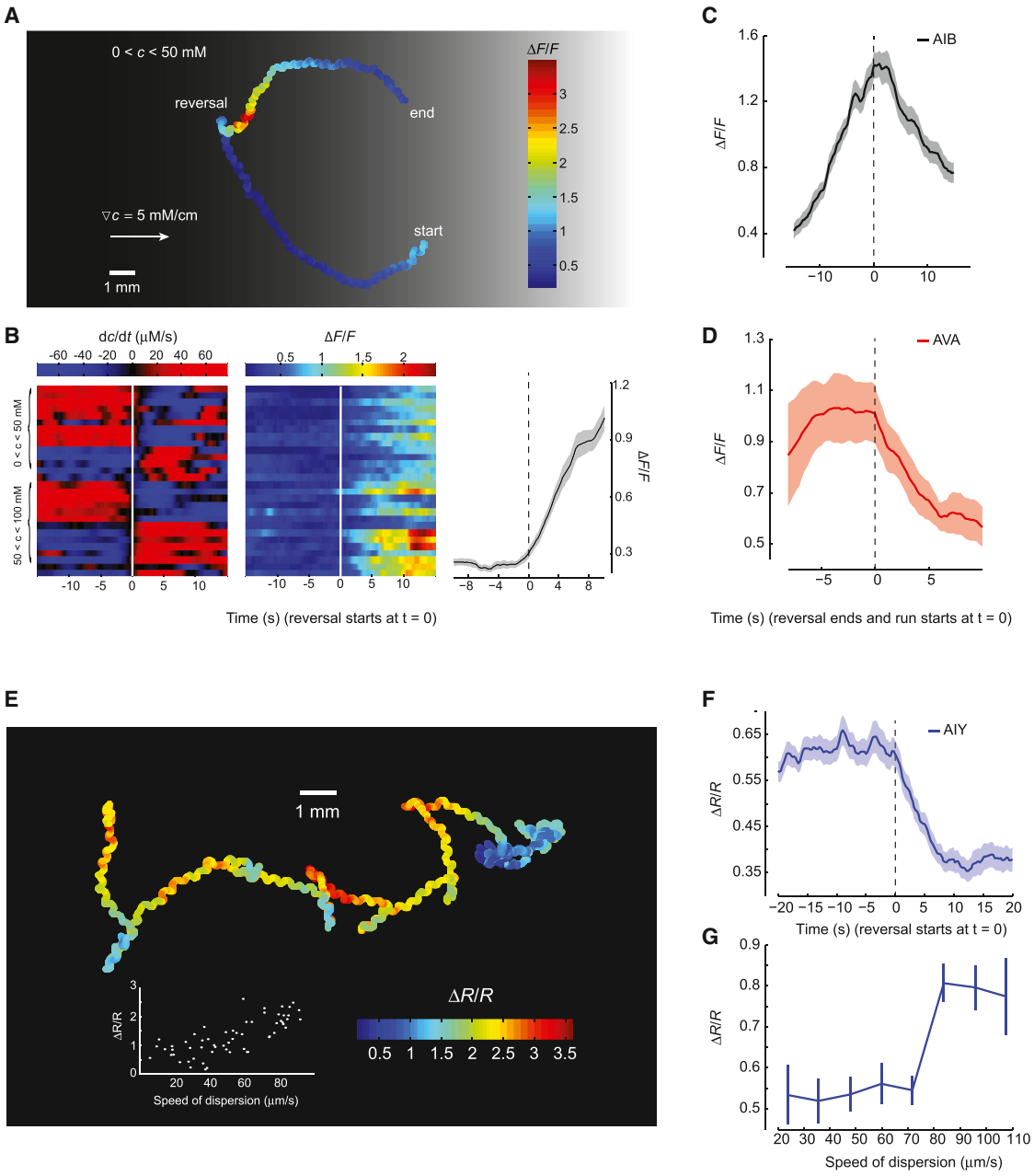

Figure 5. Calcium Imaging of Downstream Interneurons in Freely Navigating Worms

(A) Representative AIB motion trajectory and its GCaMP6 calcium signal in a worm freely navigating a linear salt gradient. AIB calcium activity increases during reversals.

(B) Heatmap of AIB calcium dynamics when *C. elegans* navigates below or above the set point (50 mM NaCl). Left and middle panels: temporal salt gradient experienced by worms during reversals (left panel, rows) and the corresponding calcium signal in AIB (middle panel). Right panel: mean values of AIB calcium signals during the onset of reversals (28 events from n = 10 animals; mean ±SEM).

(C and D) AIB (C) and AVA (D) exhibit distinct temporal calcium dynamics during reversals. Solid lines and shading represent mean ±SEM (n = 7 animals).

(E) Representative AIY motion trajectory and its ratiometric calcium signal (R) in a freely crawling worm. Inset plots the average AIY calcium signal during a 20 s course as a function of dispersion speed, defined as $\langle [r(t+\tau) - r(t)]/\tau \rangle$, where $\langle \ldots \rangle$ is the average over all t and τ within a 20 s movie.

(F) Mean values of AIY calcium signal during the onset of reversals (30 events from n = 8 animals; mean ±SEM).

(G) AIY calcium signal as a function of dispersion speed (mean ±SEM; n = 8 animals totaling ~80 min of recording). Worms with faster dispersion speed (>80 μm/s) exhibit higher AIY calcium signal (Wilcoxon rank sum test; $p < 0.000005$).

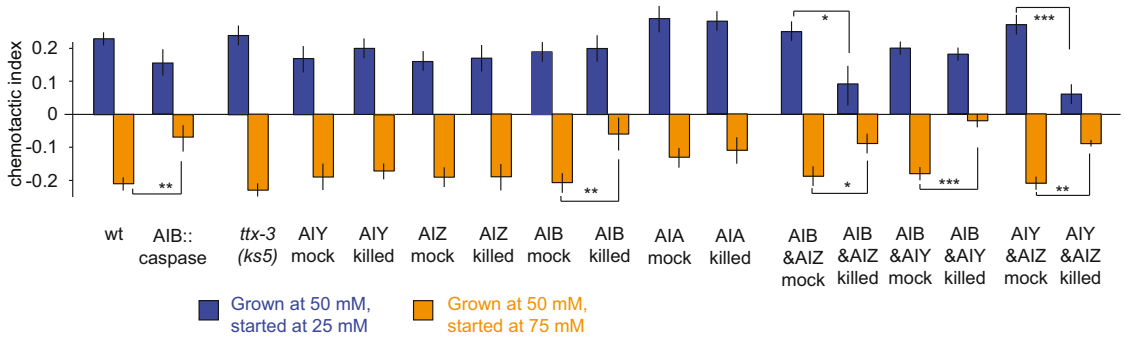

Figure 6. Downstream Interneurons Differentially Regulate Positive and Negative Chemotaxis

Chemotactic indexes of wild-type N2, mutant, and interneuron-killed animals with corresponding mock surgical controls grown at 50 mM in linear 2 mM/cm NaCl gradients starting at 25 mM (blue) or 75 mM (orange). Significant differences in the chemotactic indexes were calculated using ANOVA Tukey-Kramer post hoc for comparisons between wild-type and mutant animals. Student's t test was used to compare laser-killed animals with mock surgical controls, ***$p < 0.0005$; **$p < 0.005$; *$p < 0.05$. $n > 20$ animals for each measurement. Data points represent mean ±SEM.

when combined with AIZ ablation, also disrupted positive chemotaxis. Ablation of AIB and AIY had a similar effect as ablating AIB by itself. Taken together, these results reveal partially overlapping but different interneuron requirements for positive versus negative chemotaxis. While both AIB alone and the combination of AIY and AIZ are needed for negative chemotaxis, only the combinations of AIZ with either AIY or AIB appear critical for positive chemotaxis. As we observed from calcium dynamics in freely moving worms, the distinct activity patterns of different interneurons represent different features of navigational movement (Figure 5). Different combinations of interneurons downstream of ASER are differentially needed to regulate positive and negative chemotaxis, revealing segregation in the sensorimotor pathways for chemotactic movement in different directions at the first layer of interneurons.

We also quantified the effect of inactivating neurons by hyperpolarization caused by ectopically expressing a constitutively activated potassium channel, *twk-18*(*gf*) (Kunkel et al., 2000). We found strong consistency between our results from laser ablation and genetic inactivation of interneurons (Figure 7A). Inhibiting AIB by selective expression of *twk-18*(*gf*) disrupted negative, but not positive, chemotaxis toward a chemotactic set point at 50 mM NaCl. Inhibiting only AIY had no effect on positive or negative chemotaxis. Inhibiting both AIB and AIY disrupted negative, but not positive, chemotaxis. Inhibiting both AIB and AIZ disrupted both negative and positive chemotaxis. Inhibiting AIB, AIY, and AIZ disrupted both positive and negative chemotaxis.

Transgenic lines provided us with larger numbers of animals than laser ablation, so we could use quantitative tracking methods to assess changes in navigational strategy. We found that the klinotaxis and biased random walk strategies were differentially sensitive to interneuron ablation (Figures 7B and 7C; Experimental Procedures). Inhibiting different combinations of AIB, AIY, and AIZ essentially abolished the biased random walk strategy during positive chemotaxis (i.e., eliminating modulation of run length) and reduced the contrast in run length between movement up gradients and down gradients during negative chemotaxis, but it had no effect on the klinotaxis strategy using sharp turns. These results reveal another aspect of segregation in the sensorimotor pathways for chemotactic behavior. Interneurons immediately downstream of ASER are needed to implement the biased random walk toward the chemotactic set point. Klinotaxis is mediated by separate downstream pathways from ASER that are not directly represented in the wiring diagram.

DISCUSSION

C. elegans Exhibits Experience-Dependent Salt Chemotaxis

Sensorimotor circuits use different operational rules to decode sensory stimuli and organize motor outputs to generate behavior with adaptive values. For sensory stimuli with fixed valence, such as noxious mechanical stimuli, simple reflex arcs like those in spinal cord motor circuits allow rapid and highly stereotyped responses. The *C. elegans* wiring diagram also encodes reflexive behavioral responses, such as rapid withdrawal from mechanical stimuli (Chalfie et al., 1985). Specialized mechanosensory neurons detect gentle touch stimuli and directly regulate command neurons for forward or backward locomotion. While different temporal patterns of mechanical stimulation at different frequencies (e.g., slow poke versus buzz) appear to induce intracellular calcium changes in mechanosensory neurons with different amplitudes, they all induce calcium transients with similar temporal patterns (Suzuki et al., 2003). In the touch circuit, the activity patterns of sensory neurons and motor neurons appear to be directly coupled in reflexive responses and invariant circuit pathways (Chalfie et al., 1985). In comparison, behavioral responses to sensory inputs with context- or experience-dependent valence must be flexible. In small animals with fixed connectomes like *C. elegans*, mechanisms like neuromodulation have been shown to modulate neural circuits to generate behavioral flexibility (Bargmann and Marder, 2013). Here, we characterize a new type of behavioral flexibility in *C. elegans* for which compact representations of perception and memory are encoded in a single sensory neuron, various locomotory patterns are encoded in the downstream

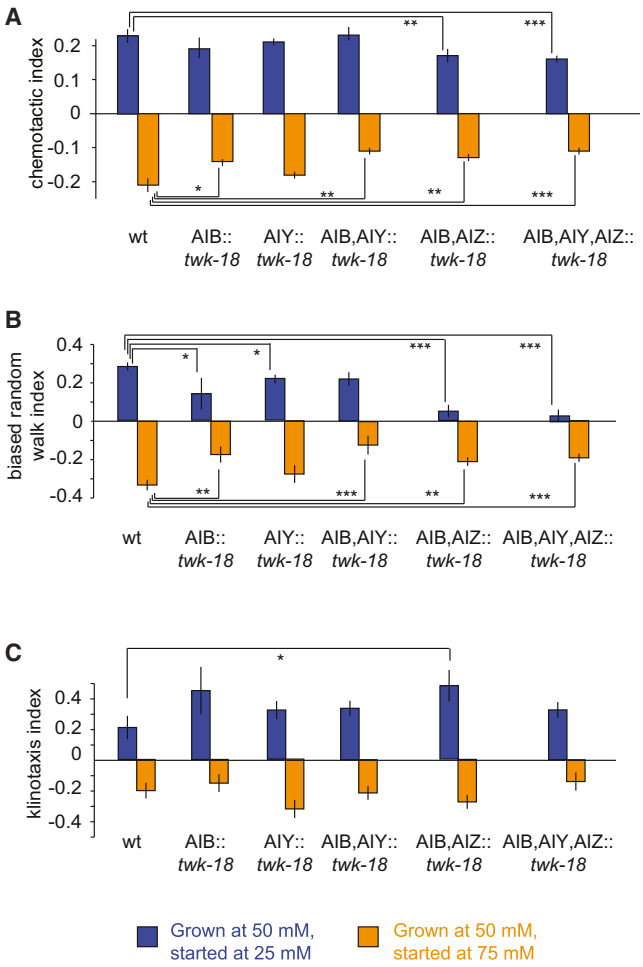

Figure 7. Downstream Interneurons Differentially Regulate the Biased Random Walk and Klinotaxis

(A–C) Chemotactic index (A), biased random walk index (B), and klinotaxis index (C) for wild-type animals and transgenic animals in which different interneurons are inhibited by ectopic expression of a constitutively active potassium channel *twk-18(gf)*. The biased random walk index was calculated as the fractional difference in the relative run durations up or down gradients $(\langle r_{up}\rangle - \langle r_{down}\rangle)/(\langle r_{up}\rangle + \langle r_{down}\rangle)$ based on the trajectories of individual animals (see Figures 2B and 2D). The klinotaxis index was calculated as the fractional difference in the relative probabilities of sharp turns reorienting the animal up or down the gradient $(\langle p_{up}\rangle - \langle p_{down}\rangle)/(\langle p_{up}\rangle + \langle p_{down}\rangle)$ as calculated based on the trajectories of individual animals (see Figures 2C and 2E). Significant differences between salient comparisons were calculated using ANOVA Tukey-Kramer post hoc; ***$p < 0.0005$; **$p < 0.005$; *$p < 0.05$; $n > 60$ animals for each measurement. Data points represent mean ±SEM.

interneurons, and rapid transformation of sensory representations to motor representations along these pathways regulate the behavioral outputs.

Previously, it was demonstrated that higher NaCl concentrations attracted *C. elegans* via a biased random walk mechanism (Pierce-Shimomura et al., 1999). Because activation of ASER is induced by downstep of NaCl and correlates with increased turning rate and activation of ASEL is induced by upstep of NaCl and correlates with decreased turning rate, the attractive response to step-increase of NaCl concentration was proposed to be a simple reflex that mapped sensory patterns to motor patterns to drive a biased random walk toward higher salt concentrations (Suzuki et al., 2008; Thiele et al., 2009). However, *C. elegans* will move either up or down smooth gradients of NaCl concentration to pursue a remembered concentration set point. Experience-dependent chemotaxis cannot be the product of fixed reflexes and requires more sophisticated information processing. As the worm navigates a gradient, it must (a) determine whether it is above or below the set point, (b) determine whether it should move up or down those gradients, and (c) select and pattern its sensorimotor responses accordingly.

ASER Encodes Sensory Stimuli and Experience with Complex Intracellular Calcium Dynamics

At the sensory level, we have shown that the ASER neuron is required for navigation up or down salt gradients as well as storing the memory of the chemotactic set point. We have also uncovered complex temporal dynamics in ASER that are both a function of gradient perception and set point memory (Figures 3 and 4). When below the set point, decreasing salt concentrations generate sustained, large-amplitude calcium waves in ASER; increasing NaCl concentration strongly suppresses ASER activity. In comparison, when above the set point, the same gradients cause ASER to exhibit sharp, discrete calcium transients; decreasing NaCl concentration evokes these sharp, discrete calcium transients with a higher frequency than increasing NaCl concentration. The richness in ASER neuronal dynamics surpasses the "ON" and "OFF" responses evoked by the step changes in NaCl concentration (Kunitomo et al., 2013; Suzuki et al., 2008). Previous studies in the visual, auditory, olfactory and somatosensory systems have shown that temporal structure of sensory activity patterns can augment information content in describing time-varying sensory inputs (Borst and Theunissen, 1999; Cury and Uchida, 2010; de Ruyter van Steveninck et al., 1997; Lu and Wang, 2004; Nagel and Wilson, 2011; Panzeri et al., 2001). The complexity of ASER neuronal dynamics may arise from its dual role in encoding perception and memory. While it is challenging to mimic the complex ASER activity patterns by manipulating neuronal activities, further investigation on causality will reveal behavioral consequence of these temporal activity patterns. By examining ASER calcium transients in freely moving worms, we were further able to show that ASER activities are not a direct representation of chemotactic movement. The sensorimotor circuit does not map ASER activity to motor activity by simple reflexes. Instead, downstream circuits must perform a more sophisticated decoding of ASER activity patterns to guide movement toward the remembered set point.

Divergent Downstream Circuits Encode Locomotory Outputs in Bidirectional Chemotaxis

To understand how experience-dependent navigation in salt chemotaxis is regulated, we asked how ASER sensory information might flow through downstream interneurons. Using laser ablation and genetic killing to remove major postsynaptic neurons of ASER—AIB, AIY and AIZ—individually and in

combination, we identified different postsynaptic neurons required for movement above or below the chemotactic set point. We found that while killing AIB or the combination of AIY and AIZ together disrupts the movement down the gradient, killing AIY and AIZ together or AIB and AIZ together is sufficient to disrupt the movement up the gradient (Figure 6). These results show that the postsynaptic interneuronal network diverges downstream of ASER, with different sets of overlapping pathways for generating positive and negative chemotaxis. Inactivating different sets of downstream interneurons in the first synaptic relay after ASER had a differential effect on the biased random walk strategy versus the klinotaxis strategy of chemotactic movement (Figure 7), highlighting another aspect of divergence in the sensorimotor pathways for chemotaxis. Thus, different memory- and perception-dependent activities of the ASER neurons must be differentially decoded by postsynaptic interneurons.

In contrast to ASER, the neuronal dynamics of major downstream interneurons—AIB, AIY, and AVA—are directly correlated with chemotactic movement but not with perception or memory (Figure 5). Interestingly, the calcium activity of each interneuron is correlated with movement, but in distinct temporal patterns. AVA activity rises to its peak near the beginning of a reorientation maneuver. AIB activity peaks at the end of each reorientation maneuver (Figures 5C and 5D). AIY calcium levels increase with forward movement, decrease with backward movement, and are thus positively correlated with dispersal rate and inversely correlated with reorientation rate (Figures 5E–5G). Thus, combinations of motor-correlated activity patterns in groups of interneurons could flexibly drive positive or negative chemotaxis. Taken together, these results suggest a highly nonlinear transformation from sensory inputs to interneurons in a condensed *C. elegans* chemotaxis circuit (Figure 1A). Furthermore, these results suggest surprisingly rapid segregation from sensory to motor representation at the first relay downstream of the principal sensory neurons.

Modeling the circuits for *C. elegans* navigation has largely involved evoking fixed sets of reflexive sensorimotor transformations, where the binary activities of sensory neurons are directly transmitted to downstream motor circuits by intervening interneurons. Mounting evidence suggests greater sophistication in the circuits for navigation than a bundle of reflexes. First, our study suggests that both perception and memory are dually represented in the complex activity patterns of the ASER sensory neuron (Figures 3 and 4). Complex temporal dynamics have been reported in other *C. elegans* sensory neurons, notably the AWC olfactory neuron, which can be activated by the sudden removal of olfactory attractants but also exhibits fast subsecond response to fluctuations in odor concentration (Kato et al., 2014) as well as spontaneous calcium activities that are both odor and temperature dependent (Biron et al., 2008; Chalasani et al., 2007). Second, our study reveals divergent sensorimotor pathways for positive versus negative chemotaxis and for regulating the frequency versus direction of reorientation movements at the first synaptic relay. Third, different interneurons in the first relay encode chemotactic movements with distinct activity patterns, suggesting rapid transformation of sensory representation to motor representation in the navigational circuit. Our results reveal that far more sophistication is compactly encoded in the navigational circuits of *C. elegans* than previously recognized.

EXPERIMENTAL PROCEDURES

Strains

Expression of G-CaMP3 (a gift from L. Tian and L. Looger at Jenelia Farm, Ashburn) in ASE was driven by the *flp-6* promoter. All worms were cultivated on nematode growth medium (NGM) plates with different NaCl concentrations and OP50 bacterial food at 20°C using standard techniques (Brenner, 1974). Other than NaCl, the composition of NGM plates is as follows: 0.25% Tryptone (w/v), 1.5% Agar (w/v), 1 mM $CaCl_2$, 1mM $MgSO_4$, 25 mM KPO_4 (pH 6.0), and 5 μg/mL cholesterol.

Behavioral Assay

Each linear gradient of NaCl was generated on a 25 cm × 25 cm plate as described in Figure S1. Osmolarity was balanced with sorbitol. Behavioral assays were performed 18–32 hr after the gradients were established. In each assay, 15–20 young adult worms were washed in NGM buffer (identical ingredients as NGM plates but without agar) for about 1 min before starting in the NaCl gradient. The assay plate was illuminated by superbright LED bars. Video was captured using a 5 megapixel USB camera (Mightex) for 15 min at 2 frames per second using Mightex Camera Demo (V1.2.0). Data was analyzed using customized particle-tracking and shape analysis algorithms written in Labview (National Instruments, Austin) and MATLAB (Mathworks, Natick). Please refer to the Supplemental Experimental Procedures for the details on data analysis.

Calcium Imaging

Calcium imaging was performed in a microfluidic device as previously described with small modifications (Chronis et al., 2007; Ha et al., 2010; Hendricks et al., 2012). Fluorescence time lapse imaging (100 ms exposures at 5 frame per second for step response or 2 frame per second for gradient response) was performed on a Nikon Eclipse Ti-U inverted microscope with a 40× oil immersion objective (NA 1.3) and a Photometrics CoolSnap EZ camera. Mean fluorescence intensities were measured with ImageJ. Animals were subjected to streams of NGM buffer containing different NaCl concentrations. Within each experiment, osmolarity was balanced with sorbitol. For gradient stimuli, a small (~400 μl) active mixing chamber driven by a magnetic stirrer was inserted inline upstream of the microfluidic device. Calibration with fluorescent dyes allowed us to adjust flow rates to achieve the desired temporal gradients, which were found to be stable and essentially linear over the imaging period. Animals were placed in the chip and exposed to either 25 mM or 75 mM NaCl for about 1 min, then exposed to either an increasing or decreasing gradient (83 ± 5 μM/s). Details on data analysis are included in the Supplemental Experimental Procedures.

Calcium imaging of freely behaving animals was performed on a Nikon Eclipse LV100 upright microscope with a 4× objective (Nikon Plan Apo NA 0.2) and an Andor iXon 885 EMCCD camera. Worms were placed on a 10 cm linear salt gradient agar plate as described in Figure S1. Ratiometric imaging was performed by splitting the red (mcherry) and green (GCaMP3 or GCaMP6) florescence signals via a dual view system (DV2, photometrics). A custom-written Labview program was used to record stage position (Ludl BioPrecision2 XY motorized stage). Fluorescence signals and worm position on the plate were analyzed using customized particle-tracking algorithms written in MATLAB.

Optogenetic Stimulation

We used our custom-built Colbert system (Leifer et al., 2011) to activate ASER neuron in a freely moving worm. Adult worms raised in 50 mM NaCl environment were transferred and immersed in 20% dextran solution (wt/vol) with 25 mM NaCl (below set point) or 75 mM NaCl (above set point). ASER neuron expressing ChR2 was activated with blue laser light (473 nm) for 6 s at a 1.5 min interval. Custom-written MATLAB scripts were used to score turning events based on how close the head and the tail of a worm are. Turning rate was

calculated by using a standard smoothing algorithm similar to the firing rate estimation in a spiking neuron (Dayan and Abbott, 2005).

SUPPLEMENTAL INFORMATION

Supplemental Information includes four figures and Supplemental Experimental Procedures and can be found with this article online at http://dx.doi.org/10.1016/j.neuron.2014.05.010.

AUTHOR CONTRIBUTIONS

L.L., Q.W., M.H., A.D.T.S., and Y.Z. conceived the experiments. L.L. performed and analyzed behavioral experiments. L.L. and Q.W. performed and analyzed optical neurophysiology in navigating worms. J.R. and M.H. performed and analyzed optical neurophysiology in microfluidics experiments. M.G., J.G., E.R.S., and M.K. contributed to behavioral tracking methods. Y.Q., H.K.S.-P., A.C.C., and D.A.C.-R. contributed reagents. L.L., Q.W., J.R., M.H., A.D.T.S., and Y.Z. interpreted results. A.D.T.S. and Y.Z. wrote the paper.

ACKNOWLEDGMENTS

We thank the *Caenorhabditis* Genetics Center (funded by National Institute of Health Office of Research Infrastructure Programs P40 OD010440) for strains, Oliver Hobert (Columbia University, New York) for the *lsy-6*(*ot71*) mutant and transgenic line expressing *otIs204* transgene, Junchao Yu for making the linear salt gradient plates, and Yuichi Iino for sharing data prior to publication. D.A.C-.R. is funded by NIH (R01NS076558). A.D.T.S. is supported by the NSF (PHY-0957185) and NIH (8DP1GM105383-05 and 1P01GM103770). Y.Z. is funded by The John Merck Fund and NIH (R01DC009852, P01GM103770). L.L. is funded by NSFC (11304153).

Accepted: April 21, 2014
Published: June 4, 2014

REFERENCES

Albrecht, D.R., and Bargmann, C.I. (2011). High-content behavioral analysis of *Caenorhabditis elegans* in precise spatiotemporal chemical environments. Nat. Methods *8*, 599–605.

Ann, K., Kowalchyk, J.A., Loyet, K.M., and Martin, T.F. (1997). Novel Ca2+-binding protein (CAPS) related to UNC-31 required for Ca2+-activated exocytosis. J. Biol. Chem. *272*, 19637–19640.

Avery, L., Bargmann, C.I., and Horvitz, H.R. (1993). The *Caenorhabditis elegans* unc-31 gene affects multiple nervous system-controlled functions. Genetics *134*, 455–464.

Bargmann, C.I., and Horvitz, H.R. (1991). Chemosensory neurons with overlapping functions direct chemotaxis to multiple chemicals in *C. elegans*. Neuron *7*, 729–742.

Bargmann, C.I., and Marder, E. (2013). From the connectome to brain function. Nat. Methods *10*, 483–490.

Biron, D., Wasserman, S., Thomas, J.H., Samuel, A.D.T., and Sengupta, P. (2008). An olfactory neuron responds stochastically to temperature and modulates *Caenorhabditis elegans* thermotactic behavior. Proc. Natl. Acad. Sci. USA *105*, 11002–11007.

Borst, A., and Theunissen, F.E. (1999). Information theory and neural coding. Nat. Neurosci. *2*, 947–957.

Boyden, E.S., Zhang, F., Bamberg, E., Nagel, G., and Deisseroth, K. (2005). Millisecond-timescale, genetically targeted optical control of neural activity. Nat. Neurosci. *8*, 1263–1268.

Brenner, S. (1974). The genetics of *Caenorhabditis elegans*. Genetics *77*, 71–94.

Chalasani, S.H., Chronis, N., Tsunozaki, M., Gray, J.M., Ramot, D., Goodman, M.B., and Bargmann, C.I. (2007). Dissecting a circuit for olfactory behaviour in *Caenorhabditis elegans*. Nature *450*, 63–70.

Chalasani, S.H., Kato, S., Albrecht, D.R., Nakagawa, T., Abbott, L.F., and Bargmann, C.I. (2010). Neuropeptide feedback modifies odor-evoked dynamics in *Caenorhabditis elegans* olfactory neurons. Nat. Neurosci. *13*, 615–621.

Chalfie, M., Sulston, J.E., White, J.G., Southgate, E., Thomson, J.N., and Brenner, S. (1985). The neural circuit for touch sensitivity in *Caenorhabditis elegans*. J. Neurosci. *5*, 956–964.

Chang, S., Johnston, R.J., Jr., and Hobert, O. (2003). A transcriptional regulatory cascade that controls left/right asymmetry in chemosensory neurons of *C. elegans*. Genes Dev. *17*, 2123–2137.

Chen, T.-W., Wardill, T.J., Sun, Y., Pulver, S.R., Renninger, S.L., Baohan, A., Schreiter, E.R., Kerr, R.A., Orger, M.B., Jayaraman, V., et al. (2013). Ultrasensitive fluorescent proteins for imaging neuronal activity. Nature *499*, 295–300.

Chronis, N., Zimmer, M., and Bargmann, C.I. (2007). Microfluidics for in vivo imaging of neuronal and behavioral activity in *Caenorhabditis elegans*. Nat. Methods *4*, 727–731.

Cury, K.M., and Uchida, N. (2010). Robust odor coding via inhalation-coupled transient activity in the mammalian olfactory bulb. Neuron *68*, 570–585.

Dayan, P., and Abbott, L.F. (2005). Theoretical Neuroscience. (MA: MIT Press).

de Ruyter van Steveninck, R.R., Lewen, G.D., Strong, S.P., Koberle, R., and Bialek, W. (1997). Reproducibility and variability in neural spike trains. Science *275*, 1805–1808.

Edwards, S.L., Charlie, N.K., Milfort, M.C., Brown, B.S., Gravlin, C.N., Knecht, J.E., and Miller, K.G. (2008). A novel molecular solution for ultraviolet light detection in *Caenorhabditis elegans*. PLoS Biol. *6*, e198.

Faumont, S., Rondeau, G., Thiele, T.R., Lawton, K.J., McCormick, K.E., Sottile, M., Griesbeck, O., Heckscher, E.S., Roberts, W.M., Doe, C.Q., and Lockery, S.R. (2011). An image-free opto-mechanical system for creating virtual environments and imaging neuronal activity in freely moving *Caenorhabditis elegans*. PLoS ONE *6*, e24666.

Gray, J.M., Hill, J.J., and Bargmann, C.I. (2005). A circuit for navigation in *Caenorhabditis elegans*. Proc. Natl. Acad. Sci. USA *102*, 3184–3191.

Ha, H.-I., Hendricks, M., Shen, Y., Gabel, C.V., Fang-Yen, C., Qin, Y., Colón-Ramos, D., Shen, K., Samuel, A.D.T., and Zhang, Y. (2010). Functional organization of a neural network for aversive olfactory learning in *Caenorhabditis elegans*. Neuron *68*, 1173–1186.

Hendricks, M., Ha, H., Maffey, N., and Zhang, Y. (2012). Compartmentalized calcium dynamics in a *C. elegans* interneuron encode head movement. Nature *487*, 99–103.

Herry, C., Ciocchi, S., Senn, V., Demmou, L., Müller, C., and Lüthi, A. (2008). Switching on and off fear by distinct neuronal circuits. Nature *454*, 600–606.

Hobert, O., Mori, I., Yamashita, Y., Honda, H., Ohshima, Y., Liu, Y., and Ruvkun, G. (1997). Regulation of interneuron function in the *C. elegans* thermoregulatory pathway by the ttx-3 LIM homeobox gene. Neuron *19*, 345–357.

Iino, Y., and Yoshida, K. (2009). Parallel use of two behavioral mechanisms for chemotaxis in *Caenorhabditis elegans*. J. Neurosci. *29*, 5370–5380.

Jansen, G., Weinkove, D., and Plasterk, R.H. (2002). The G-protein gamma subunit gpc-1 of the nematode C.elegans is involved in taste adaptation. EMBO J. *21*, 986–994.

Jing, J., and Gillette, R. (2000). Escape swim network interneurons have diverse roles in behavioral switching and putative arousal in Pleurobranchaea. J. Neurophysiol. *83*, 1346–1355.

Johnston, R.J., and Hobert, O. (2003). A microRNA controlling left/right neuronal asymmetry in *Caenorhabditis elegans*. Nature *426*, 845–849.

Kato, S., Xu, Y., Cho, C.E., Abbott, L.F., and Bargmann, C.I. (2014). Temporal responses of *C. elegans* chemosensory neurons are preserved in behavioral dynamics. Neuron *81*, 616–628.

Kerchner, G.A., and Nicoll, R.A. (2008). Silent synapses and the emergence of a postsynaptic mechanism for LTP. Nat. Rev. Neurosci. *9*, 813–825.

Kunitomo, H., Sato, H., Iwata, R., Satoh, Y., Ohno, H., Yamada, K., and Iino, Y. (2013). Concentration memory-dependent synaptic plasticity of a taste circuit

regulates salt concentration chemotaxis in *Caenorhabditis elegans*. Nat. Commun. *4*, 2210.

Kunkel, M.T., Johnstone, D.B., Thomas, J.H., and Salkoff, L. (2000). Mutants of a temperature-sensitive two-P domain potassium channel. J. Neurosci. *20*, 7517–7524.

Leifer, A.M., Fang-Yen, C., Gershow, M., Alkema, M.J., and Samuel, A.D.T. (2011). Optogenetic manipulation of neural activity in freely moving *Caenorhabditis elegans*. Nat. Methods *8*, 147–152.

Liu, J., Ward, A., Gao, J., Dong, Y., Nishio, N., Inada, H., Kang, L., Yu, Y., Ma, D., Xu, T., et al. (2010). *C. elegans* phototransduction requires a G protein-dependent cGMP pathway and a taste receptor homolog. Nat. Neurosci. *13*, 715–722.

Lu, T., and Wang, X. (2004). Information content of auditory cortical responses to time-varying acoustic stimuli. J. Neurophysiol. *91*, 301–313.

McCormick, K.E., Gaertner, B.E., Sottile, M., Phillips, P.C., and Lockery, S.R. (2011). Microfluidic devices for analysis of spatial orientation behaviors in semi-restrained *Caenorhabditis elegans*. PLoS ONE *6*, e25710.

Nagel, K.I., and Wilson, R.I. (2011). Biophysical mechanisms underlying olfactory receptor neuron dynamics. Nat. Neurosci. *14*, 208–216.

Panzeri, S., Petersen, R.S., Schultz, S.R., Lebedev, M., and Diamond, M.E. (2001). The role of spike timing in the coding of stimulus location in rat somatosensory cortex. Neuron *29*, 769–777.

Pierce-Shimomura, J.T., Morse, T.M., and Lockery, S.R. (1999). The fundamental role of pirouettes in *Caenorhabditis elegans* chemotaxis. J. Neurosci. *19*, 9557–9569.

Pierce-Shimomura, J.T., Faumont, S., Gaston, M.R., Pearson, B.J., and Lockery, S.R. (2001). The homeobox gene lim-6 is required for distinct chemosensory representations in *C. elegans*. Nature *410*, 694–698.

Ramot, D., MacInnis, B.L., Lee, H.-C., and Goodman, M.B. (2008). Thermotaxis is a robust mechanism for thermoregulation in *Caenorhabditis elegans* nematodes. J. Neurosci. *28*, 12546–12557.

Richmond, J.E., Davis, W.S., and Jorgensen, E.M. (1999). UNC-13 is required for synaptic vesicle fusion in *C. elegans*. Nat. Neurosci. *2*, 959–964.

Saeki, S., Yamamoto, M., and Iino, Y. (2001). Plasticity of chemotaxis revealed by paired presentation of a chemoattractant and starvation in the nematode *Caenorhabditis elegans*. J. Exp. Biol. *204*, 1757–1764.

Suzuki, H., Kerr, R., Bianchi, L., Frøkjaer-Jensen, C., Slone, D., Xue, J., Gerstbrein, B., Driscoll, M., and Schafer, W.R. (2003). In vivo imaging of *C. elegans* mechanosensory neurons demonstrates a specific role for the MEC-4 channel in the process of gentle touch sensation. Neuron *39*, 1005–1017.

Suzuki, H., Thiele, T.R., Faumont, S., Ezcurra, M., Lockery, S.R., and Schafer, W.R. (2008). Functional asymmetry in *Caenorhabditis elegans* taste neurons and its computational role in chemotaxis. Nature *454*, 114–117.

Thiele, T.R., Faumont, S., and Lockery, S.R. (2009). The neural network for chemotaxis to tastants in *Caenorhabditis elegans* is specialized for temporal differentiation. J. Neurosci. *29*, 11904–11911.

Tian, L., Hires, S.A., Mao, T., Huber, D., Chiappe, M.E., Chalasani, S.H., Petreanu, L., Akerboom, J., McKinney, S.A., Schreiter, E.R., et al. (2009). Imaging neural activity in worms, flies and mice with improved GCaMP calcium indicators. Nat. Methods *6*, 875–881.

Tomioka, M., Adachi, T., Suzuki, H., Kunitomo, H., Schafer, W.R., and Iino, Y. (2006). The insulin/PI 3-kinase pathway regulates salt chemotaxis learning in *Caenorhabditis elegans*. Neuron *51*, 613–625.

Tsalik, E.L., and Hobert, O. (2003). Functional mapping of neurons that control locomotory behavior in *Caenorhabditis elegans*. J. Neurobiol. *56*, 178–197.

Uchida, O., Nakano, H., Koga, M., and Ohshima, Y. (2003). The *C. elegans* che-1 gene encodes a zinc finger transcription factor required for specification of the ASE chemosensory neurons. Development *130*, 1215–1224.

Ward, S. (1973). Chemotaxis by the nematode *Caenorhabditis elegans*: identification of attractants and analysis of the response by use of mutants. Proc. Natl. Acad. Sci. USA *70*, 817–821.

White, J.G., Southgate, E., Thomson, J.N., and Brenner, S. (1986). The structure of the nervous system of the nematode *Caenorhabditis elegans*. Philos. Trans. R. Soc. Lond. B Biol. Sci. *314*, 1–340.